Journal of Applied Physics ARTICLE scitation.org/journal/jap

Features of FeB pair light-induced dissociation and repair in silicon n^+-p-p^+ structures under ultrasound loading

Cite as: J. Appl. Phys. **130**, 235703 (2021); doi: 10.1063/5.0073135
Submitted: 28 September 2021 · Accepted: 28 November 2021 ·
Published Online: 21 December 2021

O. Olikh,[1,a)] V. Kostylyov,[2] V. Vlasiuk,[2] R. Korkishko,[2] Ya. Olikh,[2] and R. Chupryna[1]

AFFILIATIONS

[1]Physics Faculty, Taras Shevchenko National University of Kyiv, Kyiv 01601, Ukraine
[2]V. Lashkaryov Institute of Semiconductor Physics of NAS of Ukraine, Kyiv 03028, Ukraine

Note: This paper is part of the Special Topic on Defects in Semiconductors.
[a)]**Author to whom correspondence should be addressed:** olegolikh@knu.ua

ABSTRACT

The experimental research in ultrasound impact on iron–boron pair transformation in silicon n^+-p-p^+ structures has revealed the decrease in concentration of pairs dissociated by light, as well as in the time of pair associations. The FeB pair changes were monitored by measuring short circuit current kinetics. The ultrasound influence was investigated at different light intensities, temperatures, frequencies, and power of acoustic waves. The possible mechanisms underlying the revealed effects were analyzed.

I. INTRODUCTION

It is widely known that the properties of semiconducting crystals and structures are determined very much by their impurity compositions. As a result, the methods aimed at modifying the system of defects are very important for practical applications. Most of these methods use irradiation, thermal treatment, or specific conditions of crystal growth. However, numerous experiments show that ultrasound also represents a sufficiently effective instrument to control the semiconductor defects. For example, it has been found that acoustic waves cause a spatial redistribution of defects,[1–6] transformation of metastable point defects,[7–9] recharging of recombination centers,[10,11] and low temperature annealing of radiation defects.[12–16] The effects of this kind are observed in silicon in particular, which is the basic modern material used in microelectronics and solar power engineering.[1,2,5,8,12,15,17,18]

The advantages of using active ultrasound (US) are the local action of elastic oscillations and the possibility to adjust the external impact by changing the type, polarization, or frequency of acoustic waves.[19] However, this method of modifying defect systems has not found wide application not least because of the lack of appropriate experimental research. In our opinion, it is most promising to use US loading (USL) as an additional factor of influence during various technological processes, which causes, in particular, the transformations in the defect system. This assumption is supported by the results obtained during ion implantation performed in the US field.[1,17,20]

Iron is an important impurity in silicon-based integrated circuit and solar cell technology. Most often, iron-related defects are the main recombination centers that determine the lifetime of minority charge carriers in particular, and device characteristics in general. Therefore, the methods aimed at iron gettering at various stocks have practical importance. There are quite many reports concerning defects of this kind. It is known that in thermal equilibrium at room temperature virtually all Fe_i is present as Fe_iB_s pairs in Si:B.[21,22] FeB pair dissociation can be accomplished by illumination at room temperature, by minority carrier injection, or by increasing the temperature.[21,23,24] Moreover, ultrasound vibrations with a frequency of 25–80 kHz and acoustic lattice strain of 10^{-5}–10^{-4} (Cz–Si[25]) or 10^{-6}–10^{-5} (poly-Si[26,27]) are capable of destroying FeB pairs. In practice, however, the most widely used technique is light-induced dissociation. The peculiarities of the dissociation and subsequent repair are well studied.[21–23,28–33] However, to the best of our knowledge, there are no reports about the US impact on these processes.

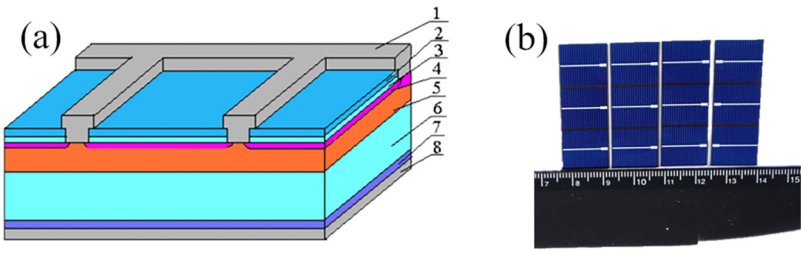

FIG. 1. (a) Scheme of the sample. (1) frontal Al electrode, (2) Si_3N_4, (3) SiO_2, (4) induced n^{++}-layer, (5) diffusion n^+-layer, (6) p-base region, (7) diffusion p^+-layer, and (8) rear Al electrode. (b) View of real solar cells; the photo was taken from the side of frontal metal electrode.

Our aim was to study experimentally the influence of ultrasound loading (2–30 MHz) on the processes of FeB $\leftrightarrow$ $Fe_i + B_s$ transformations in silicon solar cells (SCs). In order to prevent irreversible changes in the material properties, we used subthreshold intensity (strain $< 2 \times 10^{-6}$). The obtained results can be applied for subtle acoustically controlled tuning of the processes involved in iron atom gettering.

II. EXPERIMENTAL AND CALCULATION DETAILS

The n^+-p-p^+-Si samples used in the experiment are shown in Fig. 1. The structure was fabricated from a 380 μm thick p-type boron-doped Czochralski silicon wafer with [100] orientation and a resistivity of 10 Ω cm. The n^+ emitter with a sheet resistance of about 20–30 $\Omega/\square$ and a thickness of 0.7 μm was formed by phosphorus diffusion from the gas phase ($POCl_3$) at 940 °C. The anti-recombination isotype barrier was created by using p^+ layer (10–20 $\Omega/\square$, 0.6 μm) formed by boron diffusion from the gas phase (BCl_3) at 985 °C. On the front surface, the antireflective and passivating SiO_2 (30 nm) and Si_3N_4 (40 nm) layers were formed. The solid and grid Al contacts were formed by magnetron sputtering on the rear and front surfaces, respectively.

It has been found that some SC lots have significantly worse parameters compared to typical solar cells for this technological process. Additional experiments with thermal annealing at temperatures of 200 and 90 °C (the procedure is described by Tayyib *et al.*[34]) showed that a sharp drop in the photoconversion parameters value is caused by iron impurities available in the SC base at concentrations up to 4×10^{13} cm^{-3} in the SC base. It has also been found that the source of iron impurity is insufficiently pure chemicals that were used in the technological process for some SC lots. To study the effect of ultrasonic loading on the transformation of iron–boron pairs, the samples from these "bad" lots with varying degrees of iron contamination [$(0.2 - 4) \times 10^{13}$ cm^{-3}] were taken. The area of the samples used in the experiment was 1.52×1.535 cm^2.

To dissociate FeB pairs, the frontal side of the sample was illuminated with a halogen lamp with a radiation intensity W_{ill} of 0.08–0.20 W/cm^2. The illumination time t_{ill} was up to 30 s.

The FeB pair association was monitored by measuring the kinetics of short circuit current $I_{SC}(t)$ after illumination by a halogen lamp—see Fig. 2. I_{SC} was measured under SC illumination by a low-intensity monochromatic light source (light-emitting diode SN-HPIR940 nm—1 W with light wavelength $\lambda = 940$ nm). The excess carrier density Δn induced by the LED illumination was estimated by using open-circuit voltage value according to Sachenko *et al.*[35] The Δn value ($< 10^{12}$ cm^{-3}) and duty cycle while $I_{SC}(t)$ measuring (0.5%) evidence that LED illumination is weak and does not cause FeB dissociation. After illumination by the halogen lamp is terminated, FeB pairs are formed again and the starting value of I_{SC} is completely recovered.

In fact, in conditions of homogeneous carrier generation in the base, which is several minority carrier diffusion lengths L_n, the short circuit current can be described as follows:[36,37]

$$I_{SC}(t) = \frac{P_{ph}(1 - R_{ph})\, q\beta\lambda}{hc} \times \frac{\alpha_{ph}\sqrt{\mu_n kT\tau(t)/q}}{1 + \alpha_{ph}\sqrt{\mu_n kT\tau(t)/q}}, \quad (1)$$

where $\alpha_{ph} = \alpha_{ph}(T, \lambda)$ is the coefficient of light absorption, P_{ph} is the light power, R_{ph} is the coefficient of reflection, β is the coefficient of quantum yield, μ_n is the electron mobility, and τ is the minority carrier lifetime in the base. In the assumption that it is the iron-related defects that play an essential role in the recombination, the following expression can be used to estimate τ:

$$\frac{1}{\tau(t)} = \frac{1}{\tau_i} + \frac{1}{\tau_{SRH}^{Fe_i}(t)} + \frac{1}{\tau_{SRH}^{FeB}(t)} + \frac{1}{\tau_{other}}, \quad (2)$$

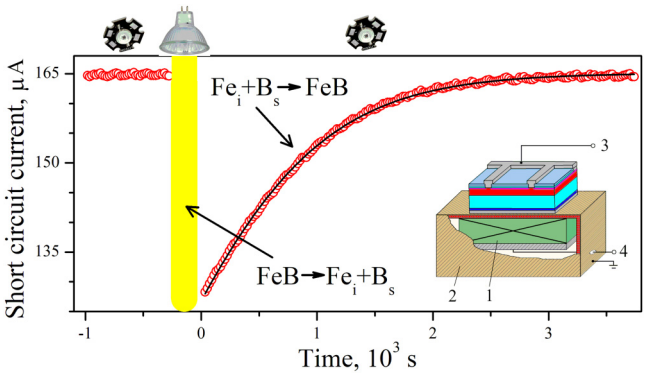

FIG. 2. Kinetics of short circuit current after intensive illumination. The marks are the experimental results, the line is the fitted curve using Eqs. (1)–(8). The zero of time corresponds to the moment of intensive illumination termination. $T = 340$ K. Inset: Scheme of USL. (1) Piezoelectric transducer, (2) metal (Cu) foil, and (3 and 4) contact to I–V measure and to ultrasound excitation, respectively.

where τ_i is the lifetime associated with intrinsic recombination; $\tau_{SRH}^{Fe_i}$ and τ_{SRH}^{FeB} are related to the recombinations at interstitial iron atoms Fe_i and at FeB pairs, accordingly; τ_{other} describes further recombination channels (other impurities, lattice defects, surface recombination). In order to calculate $\tau_{SRH}^{Fe_i}$ and τ_{SRH}^{FeB}, the Shockley–Read–Hall model was used,

$$\tau_{SRH}^{Fe_i,FeB}(t) = \frac{\tau_{p0}^{Fe_i,FeB}(t) \times (n_0 + n_1^{Fe_i,FeB} + \Delta n)}{N_A + n_0 + \Delta n} + \frac{\tau_{n0}^{Fe_i,FeB}(t) \times (N_A + p_1^{Fe_i,FeB} + \Delta n)}{N_A + n_0 + \Delta n}, \quad (3)$$

where N_A is the material's doping level ($1.4 \times 10^{15}\,cm^{-3}$), n_0 is the equilibrium electron concentration given by the law of mass action, and n_1 and p_1 are given by

$$n_1^{Fe_i,FeB} = N_C \exp\left(-\frac{E_C - E_t^{Fe_i,FeB}}{kT}\right), \quad p_1^{Fe_i,FeB} = N_V \exp\left(-\frac{E_t^{Fe_i,FeB} - E_V}{kT}\right), \quad (4)$$

where E_C and E_V are the energies of the conduction band and valence band edge, respectively, N_C and N_V are the densities of states in the conduction band and valence band, respectively, and E_t is the energy level of the relevant defect. The respective capture time constants of electrons and holes at the defect are given by

$$\tau_{p0}^{Fe_i,FeB}(t) = \frac{1}{N_{Fe,FeB}(t)\sigma_p^{Fe_i,FeB}\upsilon_{th}^p}, \quad \tau_{n0}^{Fe_i,FeB}(t) = \frac{1}{N_{Fe,FeB}(t)\sigma_n^{Fe_i,FeB}\upsilon_{th}^n}, \quad (5)$$

where $N_{Fe}(t)$ and $N_{FeB}(t)$ are the concentrations of Fe_i and FeB, respectively, υ_{th} is the thermal velocity, and σ_n and σ_p are the respective capture cross sections of electrons and holes at the defect.

The time dependence of interstitial iron atom concentration after pair dissociation is described by the known expression from Refs. 38 and 39,

$$N_{Fe}(t) = (N_{Fe,0} - N_{Fe,eq}) \times \exp(-t/\tau_{ass}) + N_{Fe,eq}, \quad (6)$$

where τ_{ass} is the characteristic time of the complex association, according to Refs. 23, 28, and 29

$$\tau_{ass} = 5.7 \times 10^5 \frac{s}{K\,cm^3} \times \frac{T}{N_A} \exp\left(\frac{E_m}{kT}\right), \quad (7)$$

where E_m is the energy of Fe_i^+ migration, $N_{Fe,0}$ is the concentration of interstitial iron atoms formed due to illumination, and $N_{Fe,eq}$ is the portion of interstitial iron atoms with $N_{Fe,0}$ that remain unpaired in the equilibrium state. According to Wijaranakula,[39] $N_{Fe,eq}$ depends on temperature, doping level, and $N_{Fe,0}$: $N_{Fe,eq} = N_{Fe,eq}(T, N_A, N_{Fe,0})$. The estimations show that at 340 K $N_{Fe,eq} \simeq 0.1 N_{Fe,0}$ for the samples under study.

In its turn, the iron–boron pair concentration N_{FeB}, which is formed as the result of the partial association of $N_{Fe,0}$, can be estimated from

$$N_{FeB}(t) + N_{Fe}(t) = N_{Fe,0}. \quad (8)$$

In case the intensive illumination causes dissociation of all the pairs, $N_{Fe,0}$ should be the same as the total concentration of the impurity iron in the structure $N_{Fe,tot}$. If the duration (or intensity) of illumination is not sufficient for total dissociation, $N_{Fe,0} < N_{Fe,tot}$. In the latter case, τ_{other} will also make contribution in the recombination of the FeB pairs that have not dissociated [with concentration $N_{Fe,tot} - N_{Fe,0} - N_{Fe,eq}(T, N_A, N_{Fe,tot} - N_{Fe,0})$] as well as the respective number of Fe_i [with concentration $N_{Fe,eq}(T, N_A, N_{Fe,tot} - N_{Fe,0})$].

In our calculations, we took $\beta = 1$, $R_{ph} = 0.14$ (the result of calculations according to Klyui *et al.*[40]), $\mu_n(T, N_A)$ from Klaassen,[41] υ_{th}^n and υ_{th}^p from Green,[42] N_C, N_V from Couderc *et al.*,[43] the defect parameters from Rougieux *et al.*,[44] and $\alpha_{ph}(T, \lambda)$ from data.[45,46] In calculating τ_i, band-to-band radiation recombination and Auger recombination were taken into account, and the temperature dependence of the corresponding coefficients was calculated according to Nguyen *et al.*[47] and Altermatt *et al.*[48] We used Eqs. (1)–(8) to fit the experimental data $I_{SC}(t)$. As fitting parameters, P_{ph}, τ_{other}, $N_{Fe,0}$, and E_m were taken. The fittings were performed by using the metaheuristic method EBLSHADE.[49]

The example of fitting results is shown in Fig. 2. In our case, the parameters determined by fitting had the following values. $P_{ph} = (3.6 \pm 0.2) \times 10^{-4}$ W, which agrees well with the value measured by PowerMeter Rk-5720 (3.5×10^{-4} W). $\tau_{other} > 100$ s, which testifies that the contribution of other recombination pathways can be neglected. $N_{Fe,0} = (1.6 \pm 0.1) \times 10^{13}\,cm^{-3}$, which is close to the value obtained for the samples of the same series from L_n measuring before and after intense illumination ($0.5 \times 10^{13}\,cm^{-3}$). In this case, L_n was measured using spectral dependencies of short circuit current[50] and the iron concentration was determined by using Zoth and Bergholz[24] equation. Finally, $E_m = (0.655 \pm 0.001)$ eV. This value coincides with that well-known value,[23,28,29,32] which is 0.66 eV. The coincidence of the values obtained by approximation with those obtained from other sources (first of all, E_m value) proves that the investigations of $I_{SC}(t)$ after intensive illumination can be applied for estimating the parameters of iron-related defects. Moreover, the peculiarities of pair dissociation (see Sec. III A) found in this way also correspond to those reported in the previous publications, which testifies that this approach is quite appropriate. In fact, the time of I_{SC} recovering is an indicator of how large the energy of migration is, and the amplitude with which I_{SC} changes in the result of intensive illumination is associated with the concentration of iron atoms released in the process. It should also be noted that this approach is similar to the method proposed by Herlufsen *et al.*,[51] in which actual concentrations of FeB pairs are estimated by the photoluminescence signal kinetics during pair association.

The measurements were carried out over a temperature range of 300–340 K. The temperature was varied by a thermoelectric cooler controlled by an STS-21 sensor and stabilized by a computer-controlled PID loop.

In the case of USL, the transverse (with frequency $f_{US} = 0.3$ MHz) or longitudinal (2–31 MHz) acoustic waves (AWs)

were applied to the samples by using a piezoelectric transducer. The US intensities W_{US} and amplitudes of strain $\xi_{US} = \sqrt{2W_{US}/\rho_{Si}\vartheta_{US}^3}$ ($\rho_{Si} = 2.33\,g/cm^3$ is the silicon density, ϑ_{US} is the US velocity, 9850 and 5840 m/s in cases of longitudinal and transverse AWs, respectively) does not overcome $1.3\,W/cm^2$ and 2×10^{-6}, respectively. Since the focus of our research was the influence of elastic vibrations on FeB pair transformations, to avoid the effect of the piezoelectric field, the transducer was shielded—see the inset of Fig. 2.

III. RESULTS AND DISCUSSION

A. FeB dissociation

In our investigation of light-induced FeB pair dissociation processes, we illuminated the structure with a halogen lamp by varying the time of illumination t_{ill} and afterward measured the kinetics of short circuit current recovery—see Fig. 3(a). As seen from the figure, the time of short circuit current recovery does not change while the amplitude of light-induced changes depends on the time of illumination. Further approximation of the experimental curves by using the approach described in the previous section allowed us to estimate the number of pairs that dissociated in the result of illumination $N_{Fe,0}$ as a function of t_{ill}. The experiments were carried out on a series of samples at different light intensities and temperatures in conditions with and without US loading. The typical results are given in Fig. 4.

The obtained results show that as the illumination time grows the values of $N_{Fe,0}$ increase gradually until reaching saturation. This is in complete correspondence with the results of the previous research studies[21,23,28] that predict the exponential decrease in pair concentration with the increase in illumination time. The saturation should correspond to the condition of complete pair dissociation. The experimentally obtained dependencies were approximated by using the following equation:

$$N_{Fe,0}(t_{ill}) = A\exp(-t_{ill}/\tau_{dis}) + N_{Fe,fit}, \tag{9}$$

where τ_{dis} is the characteristic time of dissociation and $N_{Fe,fit}$ is the value corresponding to saturation. The examples of approximation curves are given in Fig. 4, and the values of the parameters obtained by approximation are given in Table I.

On the other way, the equilibrium between free Fe_i and Fe_iB_s is determined by the following rate equations:

$$\begin{aligned} Fe_i + B_s &\xrightarrow{R_a} FeB, \\ FeB &\xrightarrow{R_d} Fe_i + B_s, \end{aligned} \tag{10}$$

where $R_a = \tau_{ass}^{-1}$ and R_d are the association and dissociation rates of FeB pairs, respectively. From Eq. (10), taking into account that $N_{Fe} = N_{Fe,tot} - N_{FeB}$ and $N_{Fe}(t_{ill} = 0) = N_{Fe,eq}$, the time-dependent interstitial iron content during illumination can be described as follows:

$$N_{Fe}(t_{ill}) = \left(N_{Fe,eq} - N_{Fe,tot}\frac{R_d}{R_d + R_a}\right)\exp[-(R_d + R_a)t_{ill}] + N_{Fe,tot}\frac{R_d}{R_d + R_a}. \tag{11}$$

The comparison of Eqs. (9) and (11) shows that $\tau_{dis}^{-1} = R_a + R_d$, $N_{Fe,fit} = N_{Fe,tot}R_d/(R_a + R_d)$. It should be noted that in our case (see Sec. III B) $\tau_{ass} \gg \tau_{dis}$ (without USL $\tau_{ass} \simeq 700$ s at 340 K and $\tau_{ass} \simeq 13\,000$ s at 300 K). Therefore, $R_d \gg R_a$ and $\tau_{dis}^{-1} \simeq R_d$, $N_{Fe,fit} \simeq N_{Fe,tot}$.

As for the case without USL, we should note the following. First, for every sample $N_{Fe,fit}$ remains constant and does not depend

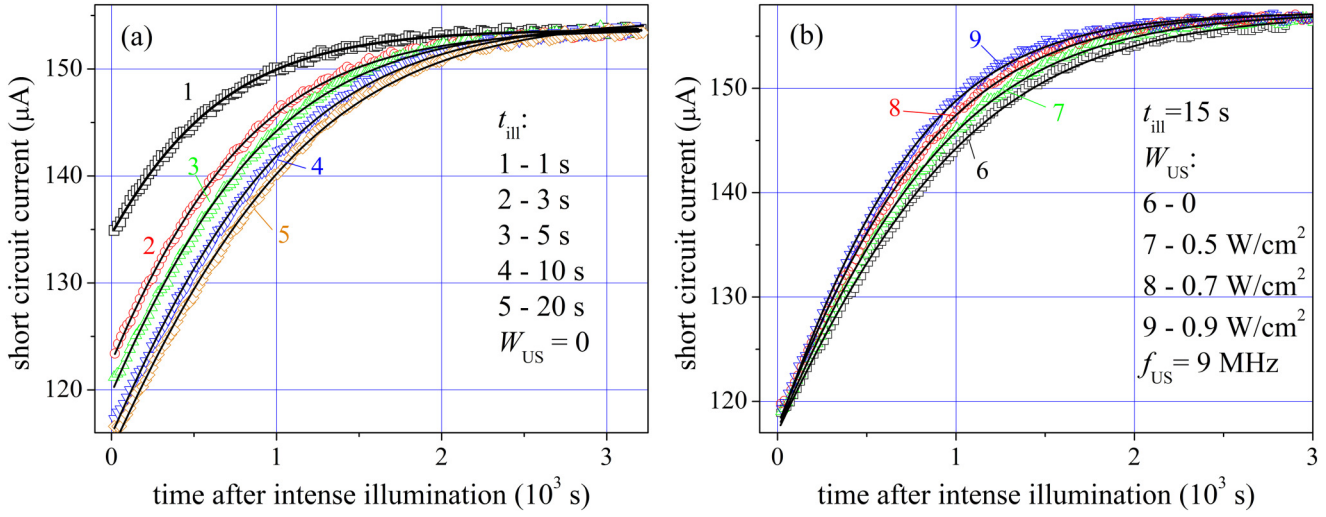

FIG. 3. Typical kinetics of short circuit current after intensive illumination of different duration (a) and USL intensity (b). The marks are the experimental results and the lines are the curves fitted by using Eqs. (1)–(8). t_{ill}, s: 1 (curve 1), 3 (2), 5 (3), 10 (4), 15 (6–9), 20 (5). W_{US}, W/cm^2: 0 (1–6), 0.5 (7), 0.7 (8), 0.9 (9). $f_{US} = 9$ MHz, $T = 340$ K.

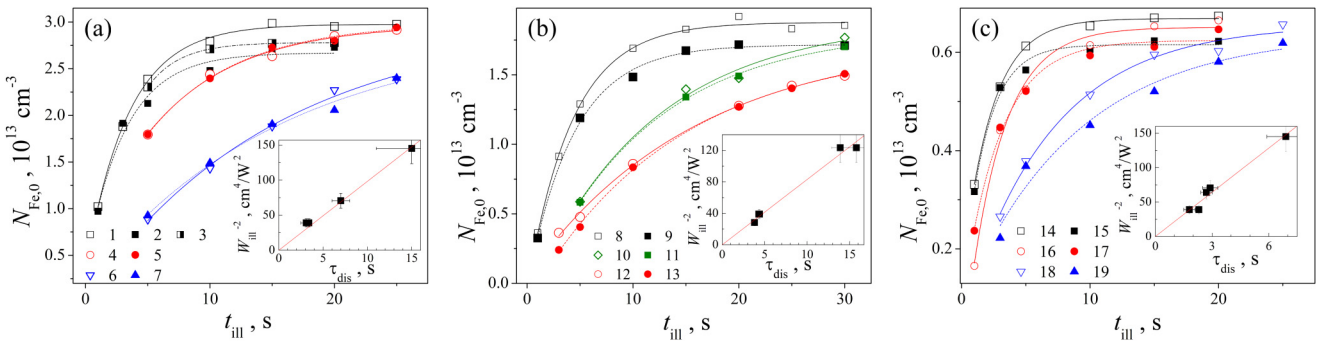

FIG. 4. Concentration dependence of interstitial atoms due to light-induced dissociation on illumination time. The marks are the experimental results and the lines are the curves fitted by using Eq. (9). Empty circles and solid lines are used for the case without USL, filled circles and dashed lines—for the case of USL. W_{ill}, W/cm^2: 0.16 (curves 1–3, 8–11, 14, 15), 0.12 (4, 5, 16, 17), 0,09 (12, 13), 0.08 (6, 7, 18, 19). W_{US}, W/cm^2: 0.9 (2, 5, 7), 0.6 (3, 9, 11, 13), 0.5 (15, 17, 19). f_{US}, MHz: 9,0 (2, 3, 5, 7), 0.3 (9, 11, 13), 5,0 (15, 17, 19); T, K: 340 (1–9, 12–19), 320 (10,11). Samples SC350-1 (a), SC350-2 (b), and SC349-1 (c). Insets: τ_{dis} are plotted against W_{ill}^{-2}. The lines are the curves fitted by $\tau_{dis} = \text{constant} \times W_{ill}^{-2}$.

on illumination intensity and temperature—see Table I. This is quite expectable if we assume that in this case $N_{Fe,fit} = N_{Fe,tot}$. Second, the value of τ_{dis} (last column in Table I) depends on W_{ill} and T. It is well known[21,28,52] that the dissociation rate of FeB pairs increases quadratically with increasing illumination intensity. In the insets of Fig. 4, the values of τ_{dis} are plotted against W_{ill}^{-2}. The linearity of the obtained curves is in complete coincidence with the reported data and can serve as an additional proof of the suggested approach applicability in estimating iron-related defect parameters. Moreover, it is known[53] that the dissociation time decreases approximately twice per 20 °C increase. In our experiment, $\tau_{dis} = (11 \pm 4)$ s for sample SC350-2 [Fig. 4(b) and Table I] at $T = 320$ K and at 340 K, it comprised 4.3 ± 0.3 s, which justifies the expectations.

Another reason why it is advisable to analyze I_{SC} kinetics is the behavior of τ_{other} revealed in the experiments. In the case when τ_{ill} corresponds to the values of $N_{Fe,0}$ close to saturation, the other recombination channels can be neglected ($\tau_{other} > 100$ ms). In the case when the values of t_{ill} are small, τ_{other} changes in the range 10^{-6}–10^{-4} s and begins to increase as the illumination time increases. In terms of the proposed approximation, this indicates that some parts of FeB pairs have not dissociated and the value of τ_{other} is related to recombination on iron-related defects that do not reconstruct when the sample is kept in darkness. In order to support this assumption, the quantity τ_{other}^{calc} was estimated as follows:

$$\tau_{other}^{calc} = \left(\left(\tau_{SRH}^{Fe_i}\right)^{-1} + \left(\tau_{SRH}^{FeB}\right)^{-1} \right)^{-1},$$

where $\tau_{SRH}^{Fe_i}$ and τ_{SRH}^{FeB} were calculated by Eq. (3) for defect concentrations $N_{Fe} = N_{Fe,eq}(N_{Fe,tot} - N_{Fe,0})$ and $N_{FeB} = N_{Fe,tot} - N_{Fe,0} - N_{Fe}$, accordingly. It turned out that τ_{other}^{calc} and τ_{other}, obtained in the same conditions, are very close: the correlation coefficient equals to 0.98 (see the supplementary material).

Paying our attention back to the impact of acoustic waves on the processes of light-induced dissociation of FeB pairs, the following should be noted. First, USL actually does not influence the magnitude of dissociation time: τ_{dis} values in neighboring rows are similar in the error range for all the cases in Table I. Second, some pairs do not dissociate under illumination in the USL case: $N_{Fe,fit}(W_{US} > 0) < N_{Fe,fit}(W_{US} = 0)$. How large the portion of these pairs is, depends on US intensity [see Figs. 4(a), Table I,

TABLE I. The value of maximum concentrations of light released iron atoms and characteristic dissociation time obtained by approximating experimental dependencies by Eq. (9).

Sample	T (K)	W_{ill} (W/cm^2)	f_{US} (MHz)	W_{US} (W/cm^2)	N_{Fe}, fit (10^{13} cm^{-3})	τ_{dis} (s)
SC350-1	340	0.08		Non	3.0 ± 0.3	15 ± 4
	340	0.08	9.0	0.9	2.9 ± 0.4	15 ± 6
	340	0.12		Non	2.98 ± 0.07	7 ± 1
	340	0.12	9.0	0.9	2.99 ± 0.06	7 ± 1
	340	0.16		Non	2.98 ± 0.02	3.4 ± 0.2
	340	0.16	9.0	0.6	2.78 ± 0.03	3.1 ± 0.6
	340	0.16	9.0	0.9	2.67 ± 0.07	2.9 ± 0.6
SC352-1	340	0.16		Non	4.25 ± 0.03	3.8 ± 0.2
	340	0.16	5.9	1.0	4.03 ± 0.04	3.7 ± 0.2
SC350-2	340	0.09		Non	1.76 ± 0.08	16 ± 2
	340	0.09	0.3	0.6	1.72 ± 0.05	14 ± 1
	340	0.12		Non	1.89 ± 0.02	9 ± 1
	340	0.12	0.3	0.6	1.86 ± 0.03	8 ± 2
	340	0.16		Non	1.88 ± 0.02	4.3 ± 0.3
	340	0.16	0.3	0.6	1.72 ± 0.02	4.4 ± 0.4
	320	0.16		Non	1.9 ± 0.2	11 ± 4
	320	0.16	0.3	0.6	1.8 ± 0.1	11 ± 1
SC349-1	340	0.08		Non	0.66 ± 0.02	7 ± 1
	340	0.08	5.0	0.5	0.64 ± 0.05	9 ± 3
	340	0.12		Non	0.65 ± 0.01	2.7 ± 0.3
	340	0.12	5.0	0.5	0.62 ± 0.01	2.9 ± 0.4
	340	0.16		Non	0.67 ± 0.01	2.3 ± 0.2
	340	0.16	5.0	0.5	0.61 ± 0.01	1.8 ± 0.3

$W_{ill} = 0.16\,W/cm^2$); at maximum W_{US} values, this portion reaches 10%. It should be noted that this [effect] is observed only in the case when light-induced pair dissociation is close to saturation. If W_{ill} (or temperature), however, is that at which a part of iron atoms stays near the substitutional boron atoms at the given illumination times, then $N_{Fe,fit}(W_{US} > 0) \simeq N_{Fe,fit}(W_{US} = 0)$.

B. FeB association

It has also been found that USL accelerates FeB pair association, see Fig. 3(b). As seen from the figure, the main result of ultrasound excitation in the structure is the decrease in time of short circuit current recovery. Since in approximating experimental dependencies $I_{SC}(t)$, we assumed that pre-exponential multiplier in Eq. (7) does not depend on USL (but relies only on the temperature and level of base doping), in order to find numerical characteristics of this effect, we used the change in migration energy ΔE_{US}, i.e., it was assumed that

$$E_m \xrightarrow{ultrasound} E_{m,0} - \Delta E_{US}, \tag{12}$$

where $E_{m,0}$ is the migration energy estimated without USL and ΔE_{US} is the acoustically induced (AI) change in migration energy. It is seen from Fig. 3(b) that ΔE_{US} depends on acoustic wave intensity. Figure 5 presents the dependencies $\Delta E_{US} = \Delta E_{US}(W_{US})$ at varied US frequencies and for the samples with different iron content (estimated by the dependencies similar to those given in Fig. 4). The presented data show that

1. ΔE_{US} shows a practically linear dependence on US intensity;
2. Effectiveness of AI change in migration energy decreases as the US frequency increases; transverse waves, despite their low frequency, less strongly impact the processes of iron ion diffusion;
3. the magnitude of AI effect practically does not depend on iron concentration;
4. AI change in migration energy can be as high as 13 meV.

ΔE_{US} has not been found to depend on illumination intensity.

The data presented in Fig. 5 were obtained at 340 K. With the decrease in temperature, the AI effect decreases—see Fig. 6. As seen from the figure, temperature dependencies of ΔE_{US} are close to linear,

$$\Delta E_{US}(T) = \Delta E_{US}(0) + \alpha_{US} T, \tag{13}$$

where temperature coefficient α_{US} depends on US frequency (see the inset of Fig. 6), while $\Delta E_{US}(0)$ depends also on the US intensity.

C. Possible mechanisms of ultrasound influence

It is obvious that the analysis of the possible reasons for US impact should be based on the mechanisms of iron-related defect transformation. It is suggested that FeB pair dissociation is a two-stage process.[21,23,54] First, the electron capture process leads to Fe_i^+ neutralization, which removes the Coulombic attraction between Fe_i^0 and B_s^-. Second, the electron capture results in the deposition of diffusion barrier energy and spatial dissociation of atoms. In the literature, two possibilities are discussed: the second electron, which leads to a negative charge state (Fe_i^-) and consequently to Coulombic

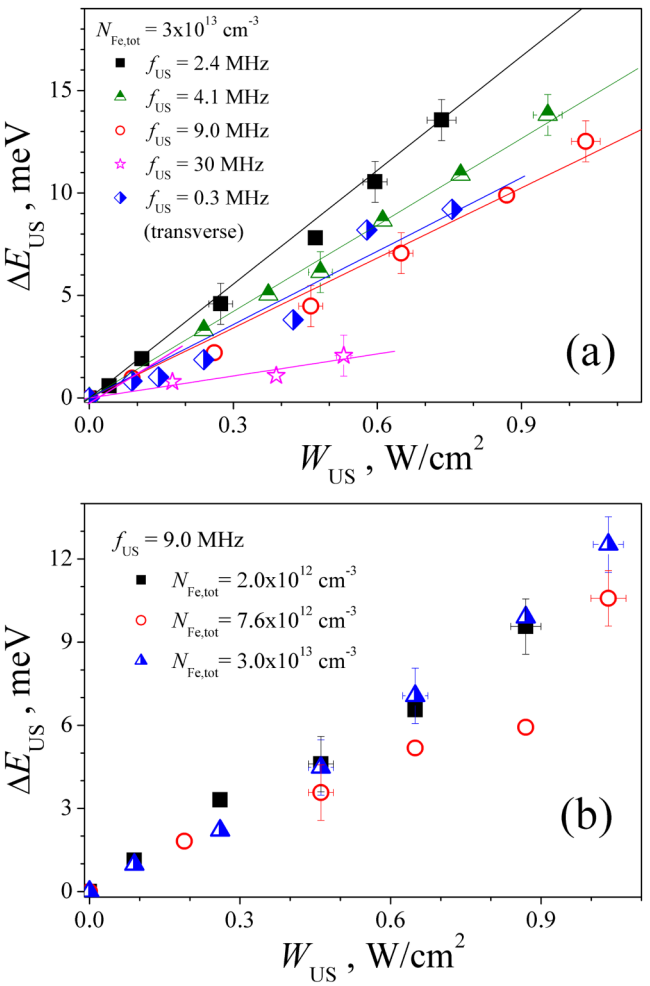

FIG. 5. Dependencies of AI change in migration energy on US intensity for various frequencies (a) and samples with different iron concentrations (b). $T = 340$ K. The points were obtained by approximating experimental dependencies and the lines are the linear fitted curves.

repulsion of $Fe_i^- B_s^-$ pair, and the second electron, which deposits the necessary Fe_i^0 migration energy after recombination with a hole. The second way is known[23] as recombination-enhanced defect reaction (REDR) and is caused by a strong electron–lattice coupling at the defect.

As for the association, it happens due to Fe_i^+ field-assisted migration to B_s^-. Therefore, a more detailed expression for τ_{ass} takes the following form:[22,23,28]

$$\tau_{ass} = \frac{\varepsilon\varepsilon_0 kT}{q^2 D_{Fe} N_A} = \frac{\varepsilon\varepsilon_0 kT}{q^2 D_{0,Fe} N_A} \exp\left(\frac{E_m}{kT}\right), \tag{14}$$

where iron diffusivity $D_{Fe} = D_{0,Fe}\exp(-E_m/kT)$, and in the general case[55–57] $D_{0,Fe} = \beta\nu a_0^2 \exp(\delta S_{Fe}/k)$, β is the correlation factor, ν is

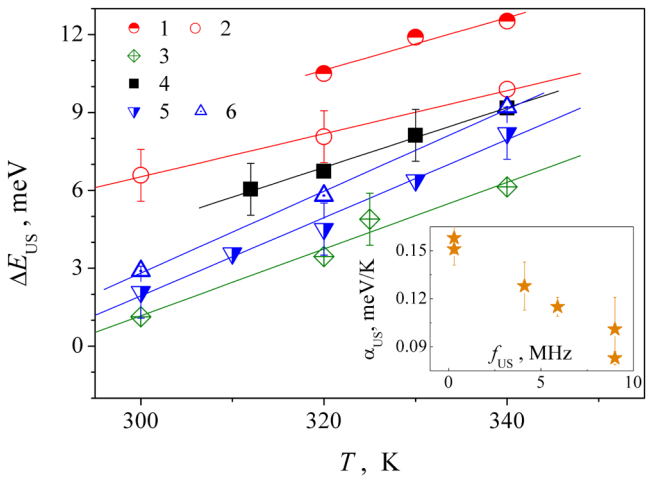

FIG. 6. Temperature dependencies of ΔE_{US}. $N_{Fe,tot}$, 10^{13} cm^{-3}: 3.0 (curves 1 and 2), 4.3 (3), 1.9 (4). f_{US}, MHz: 9.0 (1,2), 4.1 (3), 5.9 (4), 0.3 (5,6). W_{US}, W/cm^2: 1 (1), 0.87 (2), 0.48 (3), 1.0 (4), 0.58 (5), 0.76 (6). The marks are the experimental results and the lines are the linear fitted curves. Inset: Frequency dependence of temperature coefficient ΔE_{US}.

the effective vibrational (attempt) frequency, a_0 is the jump distance, and δS_{Fe} is the migration entropy.

For non-piezoelectric materials, the main effect of acoustic waves is associated with the mechanical stresses they cause. It is reported[55,58–64] about several stress-related mechanisms of impurity diffusivity variation. For instance, Aziz *et al.*[55,58] show that due to static stresses σ_{stat} in the crystal, the impurity migration energy can decrease by $\Delta E = \sigma_{stat} V^*$, where V^* is the activation strain tensor. It is known[65] that as US propagates through the crystal, it causes static strain,

$$u_{stat} = \frac{\beta}{8}\left(\frac{2\pi f_{US} u_{US}}{v_{US}}\right)^2 = \frac{\beta W_{US}}{4\rho_{Si} v_{US}^3}, \tag{15}$$

where β is the acoustic nonlinearity parameter and $u_{US} = \frac{1}{\pi f_{US}}\sqrt{\frac{W_{US}}{2\rho_{Si} v_{US}}}$ is the amplitude of lattice atom displacements. Therefore, the effect should be linear with respect to the US intensity, which correlates with the experimental data. It is known,[58,66] however, that $V^* = (0.01 - 0.2)\Omega$, where Ω is the atomic volume ($\sim 2 \times 10^{-29}$ m^3 for silicon), and the value of the multiplier depends on the kind of impurity. If we consider the propagation of longitudinal waves in direction [100] ($\beta = 2.0003$ is assumed,[67] $\sigma_{stat} = c_{11} u_{stat}$, $c_{11} = 166$ GPa), for $W_{US} = 1$ W/cm^2 we shall obtain $\Delta E = 5 \times 10^{-11}$ eV. Therefore, this mechanism cannot be the cause of the revealed effect.

According to the data,[60–62] the diffusion of impurities in US fields can occur due to elastic deformation. In particular, the energy of interaction between a single defect and the strain field is given by

$$E_{int}(x, t) = -K\Omega_d \xi(x, t), \tag{16}$$

where K is the bulk modulus (102 GPa for Si), Ω_d is the variation of crystal volume, in the result of point defect formation, for interstitial defect[61] $\Omega_d = (1.7 - 2.2)\Omega$, and ξ is the lattice relative deformation by the acoustic wave. The estimation of maximum interaction for $W_{US} = 1$ W/cm^2 yields $E_{int} \simeq 0.1$ meV. Although Baransky *et al.*[68] state that in case of clusters containing N_t defects, a collective effect can be observed, when $E_{int} \to N_t E_{int}$, in our opinion, this mechanism cannot be crucial in the effect of AI acceleration of FeB pair association revealed in our research.

In turn, the most probable cause of a decrease in τ_{ass} is the process of impurity interactions with nonequilibrium excitations of the crystal lattice described in Refs. 63 and 64, which results in the change in probability of diffusion transitions. According to Pavlovich,[63] the US influence is that it causes an increase in crystal effective temperature and an effective decrease in "polaron" activation energy. The latter is related to the transfer of lattice deformation around the impurity during diffusion transition.[63] It should be noted that according to calculations,[63] this effect should depend linearly on US intensity and temperature, which correlates with experimentally found peculiarities of AI changes. In addition, according to Krevchik *et al.*,[64] $\Delta E_{US} \sim t_s$, where t_s is phonon collision time, which can account for the revealed frequency dependence of the effect.

It should be noted that the iron–boron pairs are found[25–27] to dissociate due to ultrasound treatment. In our opinion, the reported herein and previous results have a lot in common. In fact, according to Ostapenko *et al.*,[26] Fe_i has to "jump" to the next nearest interstitial under ultrasound action; we state about the decrease in Fe_i migration energy value as well as the enhance of Fe_i diffusivity in case of ultrasound loading. Further, the efficiency of AI dissociation, as well as AI τ_{ass} fall, increases with the rise of temperature. The difference in the action of ultrasound (the iron–boron pairs dissociation or the enhancing of pairing) is associated with the difference in the intensity of the acoustic influence. For instance, the researchers used acoustic strain $\xi_{US} = 10^{-5}$–10^{-4} was used[25] to dissociate FeB pairs in Cz–Si. Furthermore, Ostapenko and Bell[25] regarded the resonance condition of pair reorientation (first step of dissociation) and used 25–70 kHz. In our case, $\xi_{US} < 2 \times 10^{-6}$ and $f_{US} = 2$–30 MHz are deficient to effectively overcome the Coulombic attraction between Fe_i^+ and B_s^-. Additionally, the presented data show that the effectiveness of acoustically induced change decreases as the ultrasound frequency increases. Besides, it should be noted that Ostapenko *et al.*[27] asserted that in the case of predominant dissociated pairs, the ultrasound treatment may promote the pairing reaction in contradistinction to the case of a high fraction of paired iron. In our case, the predominant dissociation was realized by intense illumination and then the ultrasound loading accelerated pairing. Thus, the reported results provided empirical evidence for the above-mentioned prediction.

As far as dissociation is concerned, it is worth paying attention to the possible US impact on the processes of charge carrier capture. For instance, it is suggested[19] that in conditions of USL the capture cross sections for complex defects should change

because of the change in effective distance between the components. In particular, this effect is expected to be especially substantial for the complexes whose components have Ω_d with opposite signs. This is what is observed for FeB ($\Omega_d(\mathrm{Fe}_i) > 0$, $\Omega_d(\mathrm{B}_s) < 0$) and for this reason, the complex should be acoustically active in terms of charge carrier capture. However, in our opinion, the processes of AI changes in $\sigma_{n(p)}$ should have influenced, first, the characteristic time of dissociation, but actually, the effects of this kind have not been revealed. AI increase of R_a should decrease $N_{\mathrm{Fe,fit}}$ [see Eqs. (9) and (11)]; however, this effect is leveled by the essential difference between τ_{dis} and τ_{ass}. Therefore, probably because of this reason, the US produces an impact on the second stage of dissociation. On the one hand, Korotchenkov and Grimmeiss[11] show that due to the change of impurity location concerning surrounding atoms in silicon under USL, the activation thermal energy of the carrier captured by the defect is decreased (up to about 10 meV at US intensities commensurate to those in our experiments). A similar increase in electron emission in our case should decrease the equilibrium part of negatively charged Fe ions experiencing Coulombic repulsion with B_s^-. On the other hand, it is shown[69] that USL of low intensity makes some part of the FeB pairs get rearranged in a metastable configuration with a different (orthorhombic) symmetry, in which the distance between the components is greater. At over threshold US intensities, the spatial separation of this kind results in a complete pair dissociation.[25–27] For our case, however, the important thing is that the decrease in distance weakens the Coulombic repulsion. In addition, the decrease in the concentration of pairs, which dissociate under illumination in the USL case, can be connected to a partial acoustically induced FeB dissociation. In fact, if some pairs were dissociated by ultrasound waves, which had been pre-exited in the sample with a high initial fraction of paired Fe, they cannot be dissociated under illumination. The decrease in the temperature or photon quantity leads to a reduction in the set of FeB which was modified by ultrasound or in the set of FeB which was modified by the capture of light-induced electrons, respectively. The sets cease to overlap and $N_{\mathrm{Fe,fit}}(W_{\mathrm{US}} > 0) \simeq N_{\mathrm{Fe,fit}}(W_{\mathrm{US}} = 0)$—see Table I. Finally, USL can be the cause of weakening the electron–lattice coupling at the defect as well as the REDR process as a whole.

Numerous publications, see, for example, Refs. 70–72, report that during such technological processes as temperature stimulated diffusion of dopants or the formation of an antireflection coating, iron atoms also undergo gettering. This is caused by Fe ions diffusion to various stocks. When performed in the US field, these processes, as the obtained results suggest, should improve the gettering effectiveness because of the greater volume from which Fe ions could be piled at the stocks.

IV. CONCLUSION

The experimental research of ultrasound impact on the processes of FeB pair transformation was carried out in silicon n^+-p-p^+ structures at near room temperatures. The investigation has revealed an acoustically driven decrease in the portion of FeB pairs that dissociate under the action of light as well as the decrease in Fe ion migration energies. The latter effect depends linearly on ultrasound intensity; the temperature decrease and ultrasound frequency increase reduce the acoustically induced change of migration energy. The analysis has shown that these phenomenons are caused by the interaction of impurities with nonequilibrium excitations of a crystal lattice, and acoustically driven attenuation of Coulombic repulsion, which is caused by the increase in distance between pair components and/or change in defect's charge. Thus, ultrasound can be an effective tool for controlling silicon structure characteristics.

SUPPLEMENTARY MATERIAL

See the supplementary material for the lifetime associated with further recombination channels plot [τ_{other} which was obtained by $I_{\mathrm{SC}}(t)$ fitting vs τ_{other}^{calc} which was calculated from $N_{\mathrm{Fe,0}}$ and $N_{\mathrm{Fe,fit}}$ values].

ACKNOWLEDGMENTS

The authors would like to acknowledge the financial support by National Research Foundation of Ukraine (Project No. 2020.02/0036).

DATA AVAILABILITY

The data that support the findings of this study are available from the corresponding author upon reasonable request.

REFERENCES

[1]M. Jivanescu, A. Romanyuk, and A. Stesmans, J. Appl. Phys. **107**, 114307 (2010).
[2]A. Gorb, O. Korotchenkov, O. Olikh, A. Podolian, and R. Chupryna, Solid State Electron. **165**, 107712 (2020).
[3]S. Ostapenko, Appl. Phys. A **69**, 225 (1999).
[4]B. Zaveryukhin, N. Zaveryukhina, and O. M. Tursunkulov, Tech. Phys. Lett. **28**, 752 (2002).
[5]N. Zaveryukhina, E. Zaveryukhina, S. Vlasov, and B. Zaveryukhin, Tech. Phys. Lett. **34**, 241 (2008).
[6]I. Dirnstorfer, W. Burkhardt, B. K. Meyer, S. Ostapenko, and F. Karg, Solid State Commun. **116**, 87 (2000).
[7]I. Buyanova, S. S. Ostapenko, A. Savchuk, and M. K. Sheinkman, in *Defects in Semiconductors 17*, Materials Science Forum Vol. 143, edited by H. Heinrich and W. Jantsch (Trans Tech Publications, 1993), pp. 1063–1068.
[8]I. Ostrovskii, O. Korotchenkov, O. Olikh, A. Podolyan, R. Chupryna, and M. Torres-Cisneros, J. Opt. A: Pure Appl. Opt. **3**, 82 (2001).
[9]T. Wosinski, A. Makosa, and Z. Witczak, Semicond. Sci. Technol. **9**, 2047 (1994).
[10]O. Olikh, Ultrasonics **56**, 545 (2015).
[11]O. Korotchenkov and H. Grimmeiss, Phys. Rev. B **52**, 14598 (1995).
[12]A. O. Podolian, A. B. Nadtochiy, and O. A. Korotchenkov, Tech. Phys. Lett. **38**, 405 (2012).
[13]Y. Olikh, M. Tymochko, and A. Dolgolenko, Technol. Phys. Lett. **32**, 586 (2006).
[14]I. Ostrovskii, N. Ostrovskaya, O. Korotchenkov, and J. Reidy, IEEE Trans. Nucl. Sci. **52**, 3068 (2005).
[15]P. Parchinskii, S. Vlasov, and L. Ligai, Semiconductors **40**, 808 (2006).
[16]O. Konoreva, Y. M. Olikh, M. Pinkovska, O. Radkevych, V. Tartachnyk, and V. Shlapatska, Superlattices Microstruct. **102**, 88 (2017).
[17]A. Romanyuk, P. Oelhafen, R. Kurps, and V. Melnik, Appl. Phys. Lett. **90**, 013118 (2007).
[18]O. Y. Olikh, K. V. Voytenko, and R. M. Burbelo, J. Appl. Phys. **117**, 044505 (2015).

[19]O. Y. Olikh, A. M. Gorb, R. G. Chupryna, and O. V. Pristay-Fenenkov, J. Appl. Phys. **123**, 161573 (2018).
[20]A. Romanyuk, V. Spassov, and V. Melnik, J. Appl. Phys. **99**, 034314 (2006).
[21]L. J. Geerligs and D. Macdonald, Appl. Phys. Lett. **85**, 5227 (2004).
[22]D. Macdonald, T. Roth, P. N. K. Deenapanray, K. Bothe, P. Pohl, and J. Schmidt, J. Appl. Phys. **98**, 083509 (2005).
[23]C. Möller, T. Bartel, F. Gibaja, and K. Lauer, J. Appl. Phys. **116**, 024503 (2014).
[24]G. Zoth and W. Bergholz, J. Appl. Phys. **67**, 6764 (1990).
[25]S. S. Ostapenko and R. E. Bell, J. Appl. Phys. **77**, 5458 (1995).
[26]S. S. Ostapenko, L. Jastrzebski, and B. Sopori, Semicond. Sci. Technol. **10**, 1494 (1995).
[27]S. S. Ostapenko, L. Jastrzebski, J. Lagowski, and B. Sopori, Appl. Phys. Lett. **65**, 1555 (1994).
[28]N. Khelifati, H. S. Laine, V. Vähänissi, H. Savin, F. Z. Bouamama, and D. Bouhafs, Phys. Status Solidi A **216**, 1900253 (2019).
[29]J. Tan, D. Macdonald, F. Rougieux, and A. Cuevas, Semicond. Sci. Technol. **26**, 055019 (2011).
[30]K. Lauer, C. Möller, D. Debbih, M. Auge, and D. Schulze, in *Gettering and Defect Engineering in Semiconductor Technology XVI*, Solid State Phenomena Vol. 242 (Trans Tech Publications Ltd, 2016), pp. 230–235.
[31]X. Zhu, D. Yang, X. Yu, J. He, Y. Wu, J. Vanhellemont, and D. Que, AIP Adv. **3**, 082124 (2013).
[32]D. Macdonald, A. Cuevas, and L. J. Geerligs, Appl. Phys. Lett. **92**, 202119 (2008).
[33]T. Bartel, F. Gibaja, O. Graf, D. Gross, M. Kaes, M. Heuer, F. Kirscht, C. Möller, and K. Lauer, Appl. Phys. Lett. **103**, 202109 (2013).
[34]M. Tayyib, J. Theobald, K. Peter, J. Odden, and T. Sætre, Energy Procedia **27**, 21 (2012).
[35]A. V. Sachenko, Y. V. Kryuchenko, V. P. Kostylyov, A. V. Bobyl, E. I. Terukov, S. N. Abolmasov, A. S. Abramov, D. A. Andronikov, M. Z. Shvarts, I. O. Sokolovskyi, and M. Evstigneev, J. Appl. Phys. **119**, 225702 (2016).
[36]A. Fahrenbruch and R. Bube, *Fundamentals of Solar Cells: Photovoltaic Solar Energy Conversion* (Academic Press, 1983), p. 580.
[37]M. Razeghi and A. Rogalski, J. Appl. Phys. **79**, 7433 (1996).
[38]J. D. Murphy, K. Bothe, M. Olmo, V. V. Voronkov, and R. J. Falster, J. Appl. Phys. **110**, 053713 (2011).
[39]W. Wijaranakula, J. Electrochem. Soc. **140**, 275 (1993).
[40]N. Klyui, V. Kostylyov, A. Rozhin, V. Gorbulik, V. Litovchenko, M. Voronkin, and N. Zaika, Opto-Electr. Rev. **8**, 402 (2000).
[41]D. Klaassen, Solid State Electron. **35**, 953 (1992).
[42]M. A. Green, J. Appl. Phys. **67**, 2944 (1990).
[43]R. Couderc, M. Amara, and M. Lemiti, J. Appl. Phys. **115**, 093705 (2014).
[44]F. E. Rougieux, C. Sun, and D. Macdonald, Sol. Energy Mater. Sol. Cells **187**, 263 (2018).
[45]K. Rajkanan, R. Singh, and J. Shewchun, Solid State Electron. **22**, 793 (1979).
[46]M. A. Green and M. J. Keevers, Prog. Photovoltaics: Res. Appl. **3**, 189 (1995).
[47]H. T. Nguyen, S. C. Baker-Finch, and D. Macdonald, Appl. Phys. Lett. **104**, 112105 (2014).
[48]P. P. Altermatt, J. Schmidt, G. Heiser, and A. G. Aberle, J. Appl. Phys. **82**, 4938 (1997).
[49]A. W. Mohamed, A. A. Hadi, and K. M. Jambi, Swarm Evol. Comput. **50**, 100455 (2019).
[50]E. D. Stokes and T. L. Chu, Appl. Phys. Lett. **30**, 425 (1977).
[51]S. Herlufsen, D. Macdonald, K. Bothe, and J. Schmidt, Phys. Status Solidi RRL **6**, 1 (2012).
[52]J. Schmidt, K. Bothe, V. V. Voronkov, and R. Falster, Phys. Status Solidi B **257**, 1900167 (2020).
[53]J. Lagowski, P. Edelman, A. M. Kontkiewicz, O. Milic, W. Henley, M. Dexter, L. Jastrzebski, and A. M. Hoff, Appl. Phys. Lett. **63**, 3043 (1993).
[54]L. Kimerling and J. Benton, Physica B+C **116**, 297 (1983).
[55]M. J. Aziz, Mater. Sci. Semicond. Process. **4**, 397 (2001).
[56]M. Stavola, *Identification of Defects in Semiconductors* (Academic Press, 1998).
[57]E. Weber, Appl. Phys. A **30**, 1 (1983).
[58]M. J. Aziz, Y. Zhao, H.-J. Gossmann, S. Mitha, S. P. Smith, and D. Schiferl, Phys. Rev. B **73**, 054101 (2006).
[59]B. Ziebarth, M. Mrovec, C. Elsässer, and P. Gumbsch, Phys. Rev. B **92**, 115309 (2015).
[60]F. Mirzade, J. Appl. Phys. **110**, 064906 (2011).
[61]F. K. Mirzade, J. Appl. Phys. **103**, 044904 (2008).
[62]R. Peleshchak, O. Kuzyk, and O. Dan'kiv, Ukr. J. Phys. **61**, 741 (2016).
[63]V. N. Pavlovich, Phys. Status Solidi B **180**, 97 (1993).
[64]V. D. Krevchik, R. A. Muminov, and A. Y. Yafasov, Phys. Status Solidi A **63**, K159 (1981).
[65]W. T. Yost and J. H. Cantrell, Phys. Rev. B **30**, 3221 (1984).
[66]M.-J. Chen and Y.-M. Sheu, Appl. Phys. Lett. **89**, 161908 (2006).
[67]J. Philip and M. A. Breazeale, J. Appl. Phys. **52**, 3383 (1981).
[68]P. Baransky, A. Belyaev, S. Komirenko, and N. Shevchenko, Solid State Phys. **32**, 2159 (1990).
[69]O. Y. Olikh and I. V. Ostrovskii, Phys. Solid State **44**, 1249 (2002).
[70]H. S. Laine, V. Vähänissi, A. E. Morishige, J. Hofstetter, A. Haarahiltunen, B. Lai, H. Savin, and D. P. Fenning, IEEE J. Photovoltaics **6**, 1094 (2016).
[71]V. Vähänissi, A. Haarahiltunen, H. Talvitie, M. Yli-Koski, and H. Savin, Prog. Photovoltaics: Res. Appl. **21**, 1127 (2013).
[72]T. Mchedlidze, C. Möller, K. Lauer, and J. Weber, J. Appl. Phys. **116**, 245701 (2014).